ChemComm

COMMUNICATION

View Article Online
View Journal | View Issue



Cite this: *Chem. Commun.*, 2019, **55**, 13737

Received 2nd September 2019,
Accepted 16th October 2019

DOI: 10.1039/c9cc06263g

rsc.li/chemcomm

# Stretchable, transparent and imperceptible supercapacitors based on Au@$MnO_2$ nanomesh electrodes†

Junlong Yang,[ab] Tianzeng Hong,[a] Jue Deng,[c] Yan Wang,[a] Fan Lei,[a] Jianming Zhang,[ad] Bo Yu,[e] Zhigang Wu,[f] Xinzheng Zhang[b] and Chuan Fei Guo*[a]

**A highly transparent and stretchable electrode based on a Au nanomesh, electrodeposited with a thin layer of $MnO_2$ with a transparency of 84.7% is introduced. The as-prepared transparent, stretchable, and imperceptible supercapacitor (TSPS) exhibits a specific capacitance of 0.53 mF $cm^{-2}$ and excellent bending stability, together with high stretchability (up to 160% strain).**

Flexible electronics have been developing rapidly as a rising technology because of their enormous potential applications for human–environment interactions.[1] Developing integratable, light weight, stretchable, transparent flexible electronics has been proposed to meet the increasing and urgent requirements when considering the application conditions of artificial intelligence and wearable electronic skin.[2] Generally, an integrated wearable electronic system often includes sensors, circuits, data acquisition and data transfer units, and a power supply. Huge efforts have been devoted to develop the functional parts of wearable devices, such as tactile sensors,[3] sweat sensors,[4] photodetectors,[5] temperature sensors,[6] and other sensing units. As the power source to support wearable and skin-like systems, flexible energy storage devices have a vital role in the whole flexible and wearable electronic system, thus, developing stretchable energy storage devices like supercapacitors is necessary but is still facing challenges.[7]

To construct stretchable supercapacitors, previous research mainly focused on the design of stretchable electrodes and active materials. For example, supercapacitors with wrinkled,[8] fiber shaped,[9] and rhombic shaped electrode structures,[10] and other stretchable geometries,[11] have been developed recently. The wrinkled and spring-like structures enable the supercapacitors to be highly stretchable. Besides stretchability, other considerations such as small thickness and high transparency are also important to realize highly skin-conformable and invisible stretchable supercapacitor systems,[12] because the high transparency is necessary for imperceptible integration of the wearable electronic system. Although many highly transparent supercapacitors are based on a gold network,[13] gold nanowires,[14] silver nanowires,[15] polypyrrole[16] and other active materials[17,18] have been developed, but these devices have limited mechanical stretchability. Therefore, it is highly desirable to fabricate a novel, stretchable and transparent supercapacitor with high-performance energy storage capacitance, high optical transparency as well as robust stretchability.

Here, a new approach to fabricating a supercapacitor with high stretchability and transparency using a Au and manganese dioxide ($MnO_2$) nanomesh electrode is introduced. The Au nanomesh, which was prepared by grain boundary lithography, has shown outstanding mechanical stretchability and optical transparency in previous work.[19] A thin layer of $MnO_2$ was then electrodeposited onto the Au nanomesh to ensure the high electrochemical properties and transparency. An interdigital type design was employed to construct a transparent, stretchable, ultrathin and planar supercapacitor (TSPS) device in this work because of the benefits of the thickness and the structure of 2D supercapacitors.

The typical fabrication process of the Au@$MnO_2$ nanomesh electrodes is described in the Experimental section and shown schematically in Fig. 1a. The as-prepared Au nanomesh (80 Ω $sq^{-1}$) was first transferred to a PDMS substrate. The $MnO_2$ was then electrodeposited onto the grid of the Au nanomesh to form a core–shell structure. The loading of $MnO_2$ was controlled by using the charge quantity as the terminal condition during electrodeposition

[a] *Department of Materials Science and Engineering & Centers for Mechanical Engineering Research and Education at MIT and SUSTech, Southern University of Science and Technology, Shenzhen, Guangdong 518055, China. E-mail: guocf@sustech.edu.cn*
[b] *School of Physics and TEDA Institute of Applied Physics, Nankai University, Tianjin 300071, China*
[c] *Department of Mechanical Engineering, Massachusetts Institute of Technology, Cambridge, MA 02139, USA*
[d] *Academy for Advanced Interdisciplinary Studies, Southern University of Science and Technology, Shenzhen, Guangdong 518055, China*
[e] *Ningbo Fengcheng Advanced Energy Materials Research Institute, Ningbo, Zhejiang, 315500, China*
[f] *State Key Laboratory of Digital Manufacturing Equipment and Technology, Huazhong University of Science and Technology, Wuhan, Hubei 430074, China*
† Electronic supplementary information (ESI) available. See DOI: 10.1039/c9cc06263g

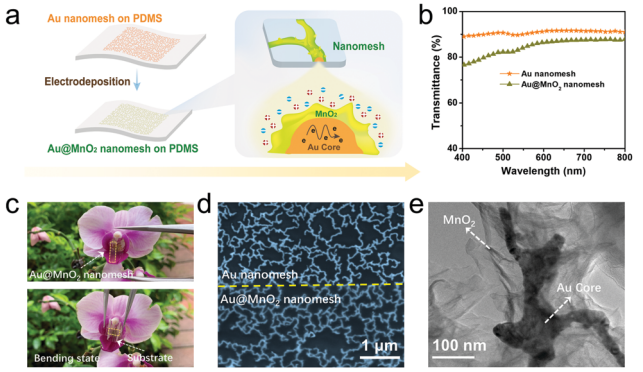


Fig. 1 (a) A schematic illustration of the fabrication of the Au@$MnO_2$ nanomesh on a PDMS substrate, and the core–shell structure of the Au@$MnO_2$ nanomesh electrode showing the ion diffusion pathways and charge transport channels. (b) Transmittance spectra of the Au nanomesh and the Au@$MnO_2$ nanomesh (0.008 C $cm^{-2}$). (c) Photographs of an Au@$MnO_2$ nanomesh electrode on a PDMS substrate in unfolded and bending states. (d) SEM images of the Au nanomesh and the Au@$MnO_2$ nanomesh. (e) A TEM image of $MnO_2$ flakes on the Au nanomesh core.

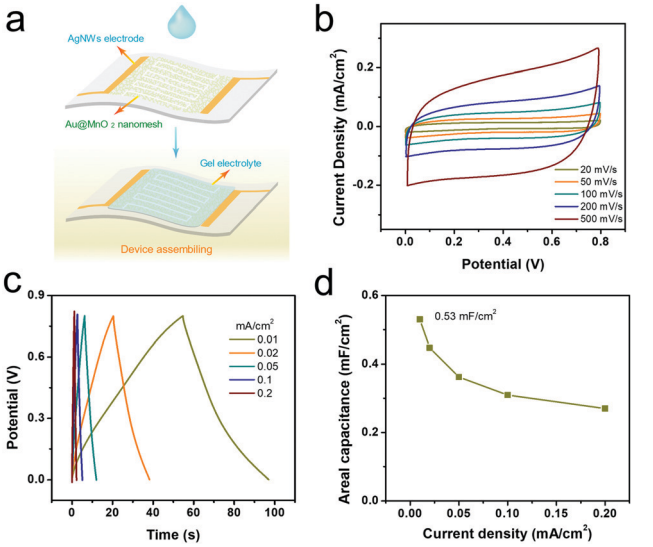


Fig. 2 (a) A schematic illustration of the device assembly of a transparent, stretchable and planar supercapacitor (TSPS) based on Au@$MnO_2$ nanomesh electrodes. (b) CV curves of the TSPS device at different scan rates. (c and d) Galvanostatic CD curves and the dependent areal capacitance of the TSPS device at different current densities.

to verify the relationship between performance and transparency, and the charge quantities tested were: 0.004 C $cm^{-2}$, 0.008 C $cm^{-2}$ and 0.016 C $cm^{-2}$.

The morphology of the Au nanomesh and the Au@$MnO_2$ nanomesh was investigated by scanning electron microscopy (SEM) and transmission electron microscopy (TEM). As shown in Fig. 1d, a clear boundary can be observed between the Au mesh and the Au@$MnO_2$ nanomesh. The continuous nanomesh of petal-shaped $MnO_2$ is coated on the surface of the Au core and its thickness increases when using a high charge quantity as the terminal condition (Fig. S1, ESI†). The TEM image further verifies that the $MnO_2$ flakes on the grid of Au nanomesh have a wrinkled morphology with a very thin thickness (Fig. 1e). The thickness of the $MnO_2$ layer is about 7 nm with a charge quantity of 0.008 C $cm^{-2}$ when the $MnO_2$ is considered to be a continuous layer (see the calculation details in the ESI†). Such a thin nanosheet enables $MnO_2$ to be mechanically flexible and also highly transparent. As shown in Fig. 1b, the transmittance of the Au@$MnO_2$ nanomesh is 84.7% at 550 nm, which offers a strong possibility for the fabrication of an invisible and imperceptible device (demonstrated from Fig. 1c). Meanwhile, the *d*-spacing sequences for the $MnO_2$ flakes are 0.241, 0.228, and 0.152 nm indexed to the interlayer spacings of the (0 1 1), (0 −1 1) and (0 1 4) planes, respectively, and these are obtained from the high resolution TEM and corresponding SAED patterns (Fig. S2, ESI†), indicating that birnessite-type $MnO_2$ was formed during electrodeposition.[20] In addition, the surface feature of the Au@$MnO_2$ nanomesh electrode was found to be hydrophilic after loading with $MnO_2$ (Fig. S3, ESI†). The Au@$MnO_2$ nanomesh electrode exhibits an areal capacitance of 1.52 mF $cm^{-2}$ at a current density of 0.0125 mA $cm^{-2}$ in a three-electrode system, and this remains at about 98% after 10 000 galvanostatic charge–discharge (GCD) cycles at a current density of 0.125 mA $cm^{-2}$, suggesting excellent capacitive performance and long-term stability (Fig. S4, ESI†).

Planar supercapacitors constructed on a single substrate have shown excellent advantages such as being separator-free, having a high-power density and ultralong life span.[21] This offers a strong possibility of fabricating competitive miniaturized energy source devices, especially for multifunctional applications. Herein, the development, and further exploration of its advantages, of an all-solid, transparent and planar supercapacitor device based on the Au@$MnO_2$ nanomesh electrodes is reported. Three planar supercapacitor devices were assembled, which included different types of interdigital fingers of the Au@$MnO_2$ nanomesh electrodes with a symmetrical structure (see the schematics in Fig. 2a and Fig. S6a, ESI†). As determined from the CV measurements (Fig. S6b, ESI†), the interdigital supercapacitor has the highest area capacitance, indicating that more finger electrodes will result in a higher performance. Therefore, this interdigital design was employed to fabricate a transparent, stretchable and planar supercapacitor (TSPS). The gap between two fingers is about 50 μm, and the width of each finger is about 600 μm for the interdigital electrodes shown in Fig. S7 (ESI†). The transparency of the TSPS device with a solid-state electrolyte remains at 82.1% at 550 nm, indicating an outstanding optical performance (Fig. S8, ESI†).

It is worth noting that the TSPS device obtained is ultra-thin because it takes advantage of the small thickness of the Au@$MnO_2$ nanomesh electrodes (~47 nm except for the electrolyte), while the thickness of the flexible substrate can be ignored. The electrochemical performance of the TSPS device was investigated using CV and GCD measurements in a two-electrode system. As shown in Fig. 2b and c, the nearly rectangular shapes and symmetry of the CV scans (even at a high scan rate of 500 mV $s^{-1}$) and nearly triangular shaped GCD curves indicate its pseudocapacitive nature. The calculated highest areal capacitance of the TSPS device from the discharge slope after the IR drop is 0.53 mF $cm^{-2}$ at 0.01 mA $cm^{-2}$ current density, which corresponds

 

to the energy density of 0.047 μW h $cm^{-2}$ at a power density of 2.16 μW $cm^{-2}$, and it decreases to 0.27 mF $cm^{-2}$ at 0.2 mA $cm^{-2}$, and the areal capacitance still remains at 51%.

A transparent wristband integrated with the TSPS device was fabricated to exhibit the potential application for wearable electronics due to its high transparency and flexibility (shown in Fig. 3a). The flexibility of the TSPS device was evaluated in terms of bending and stretching performance. As shown in Fig. 3b and c, no obvious change is observed in the CV curves after bending at curvature radii from 1.7 to 5.0 mm at a scan rate of 200 mV $s^{-1}$ (the digital photos at the bending state are shown in Fig. S9, ESI†). The specific capacitance maintained by near 100% of its initial capacitance after 200 cycles of bending/releasing at a bending radius of 2 mm (Fig. 3d), suggested that the TSPS device had a high bending stability. Meanwhile, the specific capacitance retained 90% of its initial value at a strain of 40% (Fig. 3e and i). Even stretched to 60% strain, the TSPS device still retained 75% of its initial capacitance. The specific capacitance of the TSPS device is nearly unchanged after stretching and releasing over 400 cycles under a strain of 40%, indicating that there is a high stretching stability. Note that human skin can typically be stretched to 20%,[1] smaller than the strains tested here. The stretchability of the TSPS device is expected to enable applications in wearable systems as well as for on skin electronics.

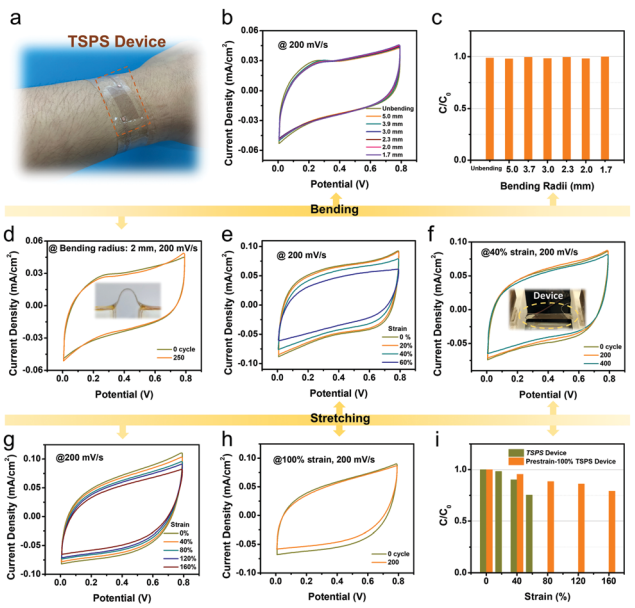


Fig. 3 (a) A wearable and transparent wristband integrated with the TSPS device. (b) CV curves of the TSPS device at different bending radii. (c) Capacitance changes at different bending radii. (d) The cycling stability of the TSPS device under a bending radius of 2 mm at a 200 mV $s^{-1}$ scan rate. (e) CV curves of the TSPS device under different stretching strains. (f) The cycling stability of the TSPS device under a tensile strain of 40% at a 200 mV $s^{-1}$ scan rate. (g) CV curves of a TSPS device with a pre-strain of 100% tested at different tensile strains. (h) The stability of the pre-strained TSPS device repeatedly stretched to a strain of 40% over 200 cycles. (i) The capacitance changes of TSPS devices without pre-strain and with 100% pre-strain, tested at different tensile strains.

However, considering other specific applications like soft robotics, even higher stretchability is demanded for the energy devices.[22] Using a pre-stretched substrate is an effective way to improve the stretchability for various electrodes by generating wrinkled structures.[23] Thus, this pre-stretching method was applied to the Au@$MnO_2$ nanomesh electrodes to further improve the stretchability. Fig. 3g shows that the specific capacitance was still retained at ~79%, even if the TSPS device (pre-strain ~100%) was stretched to a strain of 160%, and the pre-strained TSPS device also exhibited excellent stability of electrochemical performance after 200 cycles of stretching at a strain of 100% (Fig. 3h and i), indicating the remarkable stability over the stretching cycles.

As demonstrated from the presented data, the TSPS device based on the Au@$MnO_2$ nanomesh electrodes exhibits high transparency (~82.1% at 550 nm) and excellent mechanical performance, without a significant decrease in capacitance when highly stretched to strains up to 160%. The high transparency lies in the network structure of the Au nanomesh and ultra-small thickness of the $MnO_2$ flakes. The thin layer of $MnO_2$ is expected to be flexible because nanoscale materials can basically generate quite small strains during bending. The large stretchability of the Au@$MnO_2$ nanomesh, however, is attributed to the Au nanomesh rather than the $MnO_2$ nanoflakes. Fig. S10 (ESI†) shows that the conductivity of the Au nanomesh increases only once when applying 100% strain. This high stretchability results from two stages of deformation of the Au nanomesh. At small strains, ligaments of the Au nanomesh are straightened, and deform out-of-plane so that the mesh pores can be elongated elastically. Beyond the elastic regime, however, some straightened nanowires break and form distributed cracks,[19] which is verified in the SEM observation in Fig. 4a. Such delocalized or distributed rupture is quite different from the failure of a free-standing film: once a crack is formed in a free-standing film it will propagate rapidly, and the film breaks into two pieces. Therefore, the elastomeric substrate plays an important role to stabilize the formed cracks and allow other places to break. Although having small distributed pockets during stretching, the Au@$MnO_2$ nanomesh remains a continuous network and keeps its the electrochemical properties. However, when much thicker $MnO_2$ is deposited on the Au nanomesh, the composite will strongly adhere to the substrate, and the improved adhesion will have a "stiffening effect" on the film,[24] and as a result, the Au@$MnO_2$ composite seriously cracks and becomes nonconducting upon stretching (Fig. S1c, ESI†). This is the reason that only a thin $MnO_2$ layer was deposited on the Au nanomesh in this work.

Generally, it is difficult for a material to realize high stretchability and high optical transparency simultaneously. Here the Au@$MnO_2$ nanomesh electrodes accommodates the previously mentioned properties well. The TSPS device has shown significant potential for applications for wearable electronics. For this device, the achieved transparency of the device is 82.1%, the specific capacitance is 0.53 mF $cm^{-2}$, and the maximum strain tested can achieve 160%, whereas the specific capacitance still remains at 79%. The transparency, specific capacitance, and stretchability of the reported supercapacitors and these devices

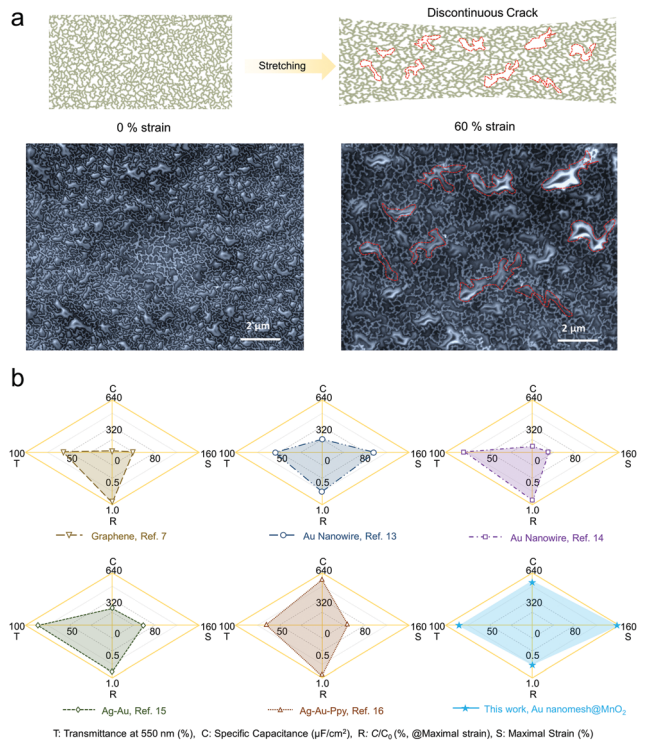


Fig. 4 (a) SEM images of Au@$MnO_2$ nanomesh under 0% strain and 60% strain, and schematic diagrams illustrating the microstructures of the Au nanomesh electrode before and after stretching, forming distributed cracks in the strained state to ensure high stretchability. (b) A comparison of the transparent and stretchable supercapacitor with recently reported supercapacitors, with transmittance at 550 nm, and showing capacitance per unit area, maximal stretchability, and the remaining capacitance at maximal strain.

are compared in Fig. 4b,[8,13–16] and detailed data are also listed in Table S1 (ESI†), including those that are only transparent[17,25,26] or stretchable.[18] Meanwhile, it can be seen that this TSPS device exhibits the highest stretchability with a stable electrochemical performance and transparency.

In conclusion, a transparent, stretchable, and ultrathin planar supercapacitor (TSPS) device has been achieved based on the interdigital design of a Au@$MnO_2$ nanomesh electrode. The TSPS displays high transparency of 82.1%, a specific capacitance of 0.53 mF $cm^{-2}$, excellent bending stability and high stretchability, allowing the device to be strained up to 60% while the specific capacitance can be maintained at 75%. When applying a pre-strain of 100% to the Au@$MnO_2$ nanomesh electrode, it can be stretched up to 160% while the specific capacitance is maintained at 79%. This work provides an effective strategy for developing stretchable and invisible electronic devices.

This work was financially supported by the funds of the National Natural Science Foundation of China (No. 51771089 and U1613204), the Guangdong Innovative and Entrepreneurial Research Team Program (2016ZT06G587), the Shenzhen DRC Project [2018]1433, the Science Technology and Innovation Committee of Shenzhen Municipality (Grant No. JCYJ20170817111714314 and JCYJ20160613160524999), and the Shenzhen Sci-Tech Fund No. KYTDPT20181011104007.

## Conflicts of interest

There are no conflicts to declare.

## Notes and references

1 K. Kim, Y. G. Park, B. G. Hyun, M. Choi and J. U. Park, *Adv. Mater.*, 2019, **31**, 1804690.
2 T. Q. Trung and N. E. Lee, *Adv. Mater.*, 2017, **29**, 1603167.
3 Y. Wan, Y. Wang and C. F. Guo, *Mater. Today Phys.*, 2017, **1**, 61–73.
4 J. Choi, R. Ghaffari, L. B. Baker and J. A. Rogers, *Sci. Adv.*, 2018, **4**, eaar3921.
5 W. Tian, C. Zhang, T. Zhai, S. L. Li, X. Wang, J. Liu, X. Jie, D. Liu, M. Liao and Y. Koide, *Adv. Mater.*, 2014, **26**, 3088–3093.
6 T. Q. Trung, S. Ramasundaram, B. U. Hwang and N. E. Lee, *Adv. Mater.*, 2016, **28**, 502–509.
7 X. Chen, H. Lin, P. Chen, G. Guan, J. Deng and H. Peng, *Adv. Mater.*, 2014, **26**, 4444–4449.
8 T. Chen, Y. Xue, A. K. Roy and L. Dai, *ACS Nano*, 2013, **8**, 1039–1046.
9 J. Sun, Y. Huang, C. Fu, Z. Wang, Y. Huang, M. Zhu, C. Zhi and H. Hu, *Nano Energy*, 2016, **27**, 230–237.
10 J. Pu, X. Wang, R. Xu and K. Komvopoulos, *ACS Nano*, 2016, **10**, 9306–9315.
11 Y. Lim, J. Yoon, J. Yun, D. Kim, S. Y. Hong, S.-J. Lee, G. Zi and J. S. Ha, *ACS Nano*, 2014, **8**, 11639–11650.
12 T. An and W. Cheng, *J. Mater. Chem. A*, 2018, **6**, 15478–15494.
13 Y. Wang, S. Gong, D. Dong, Y. Zhao, L. W. Yap, Q. Shi, T. An, Y. Ling, G. P. Simon and W. Cheng, *Nanoscale*, 2018, **10**, 15948–15955.
14 S. Gong, Y. Zhao, Q. Shi, Y. Wang, L. W. Yap and W. Cheng, *Electroanalysis*, 2016, **28**, 1298–1304.
15 H. Lee, S. Hong, J. Lee, Y. D. Suh, J. Kwon, H. Moon, H. Kim, J. Yeo and S. H. Ko, *ACS Appl. Mater. Interfaces*, 2016, **8**, 15449–15458.
16 H. Moon, H. Lee, J. Kwon, Y. D. Suh, D. K. Kim, I. Ha, J. Yeo, S. Hong and S. H. Ko, *Sci. Rep.*, 2017, **7**, 41981.
17 S. B. Singh, T. Kshetri, T. I. Singh, N. H. Kim and J. H. Lee, *Chem. Eng. J.*, 2019, **359**, 197–207.
18 P. Xu, B. Wei, Z. Cao, J. Zheng, K. Gong, F. Li, J. Yu, Q. Li, W. Lu and J.-H. Byun, *ACS Nano*, 2015, **9**, 6088–6096.
19 C. F. Guo, T. Sun, Q. Liu, Z. Suo and Z. Ren, *Nat. Commun.*, 2014, **5**, 3121.
20 S. Devaraj and N. Munichandraiah, *J. Phys. Chem. C*, 2008, **112**, 4406–4417.
21 P. Zhang, F. Wang, M. Yu, X. Zhuang and X. Feng, *Chem. Soc. Rev.*, 2018, **47**, 7426–7451.
22 G. M. Whitesides, *Angew. Chem., Int. Ed.*, 2018, **57**, 4258–4273.
23 Y. Wang, Q. Liu, J. Zhang, T. Hong, W. Sun, L. Tang, E. Arnold, Z. Suo, W. Hong and Z. Ren, *Adv. Mater.*, 2019, 1902955.
24 C. F. Guo, Y. Chen, L. Tang, F. Wang and Z. Ren, *Nano Lett.*, 2015, **16**, 594–600.
25 S. Kiruthika, C. Sow and G. Kulkarni, *Small*, 2017, **13**, 1701906.
26 T. Qiu, B. Luo, M. Giersig, E. M. Akinoglu, L. Hao, X. Wang, L. Shi, M. Jin and L. Zhi, *Small*, 2014, **10**, 4136–4141.

 